7.4 EXPLORATION OF THE RADIATION RESISTANCE OF HIGH ENTROPY ALLOYS — C. Li, S.J. Zinkle (University of Tennessee), N.A.P. Kiran Kumar, H. Bei (ORNL)

OBJECTIVE

The goal of this project is exploring the basic radiation resistance of high entropy alloys (HEAs) that may have the potential for very good resistance to radiation-induced property degradation.

SUMMARY

This report summarizes the experimental characterization of neutron and ion irradiated 27%Fe-27%Mn-28%Ni-18%Cr HEA. Samples have been neutron irradiated at ~70˚C from 0.1 dpa to 1 dpa, and ion irradiated with 5.8 MeV Ni ions at temperatures ranging from 400˚C to 700˚C and midrange doses from 0.1 dpa to 10 dpa. Post irradiation examination of the neutron irradiated samples found a large increase of hardness after 0.1 dpa, whereas there was only a mild increase from 0.1dpa to 1dpa. Similar trend was observed with the change of yield strength and electrical resistivity. The stress-strain curves of the neutron irradiated specimens are in agreement with the typical behavior of 304, 316 and 347 austenitic stainless steels, but the large yield drop and reduction of work hardening rate seems to be unique to HEA. Ion irradiations at higher temperatures showed evidence of sluggish diffusion with almost no solute depletion or enrichment at grain boundaries. Voids were also not observed at any irradiation condition, suggests that this type of HEA is fairly stable under high temperature radiation.

PROGRESS AND STATUS

Introduction

HEAs consist of four or more elements with nearly equimolar ratios, giving rise to high configurational entropy. HEAs can be either face centered cubic (f.c.c) or body centered cubic (b.c.c) phases without formation of brittle phases that frequently observed in conventional simple intermetallic alloys[1-5]. Due to their superior mechanical properties, HEAs have potential application as a structural material in advanced nuclear energy systems. However, little is known about their stability under neutron or ion irradiation. It is hypothesized that the high configurational entropy might modify point defect (solute and radiation-induced point defects) diffusion, recombination and agglomeration processes.

Austenitic steels are widely used in current nuclear fission reactors and are proposed for advanced fission reactors and fusion reactor first-wall structures such as ITER[6]. However, they don't appear to show sufficient radiation resistance required for the extended operation of current fission reactors or advanced reactor concepts. Of all the radiation degradation phenomena in Fe-based austenitic steels, void swelling and radiation-induced segregation (RIS) are two extremely significant challenges.

In the current study, a novel 27%Fe-27%Mn-28%Ni-18%Cr single phase f.c.c HEA has been characterized after ion and neutron irradiation. The objective of this study is to examine the change of mechanical properties and microstructure of this HEA after irradiation over a wide range of irradiation temperatures.

Experimental Procedure

Many of the high entropy alloys studied to date contain Co, making them unfavorable for nuclear applications due to neutron activation. In the present study, a novel 27%Fe-27%Mn-28%Ni-18%Cr high entropy alloy has been synthesized. The material was prepared by arc-melting by mixing constituent metals of high purity. The cast bar was then homogenized at 1200°C for 48 h, cold rolled and recrystallized at 900°C for 4hr in a vacuum furnace to obtain fully recrystallized microstructure.
For neutron irradiation, samples were irradiated at ~70 ˚C from 0.1 dpa to 1 dpa in the High Flux Isotope Reactor (HFIR). Six SS3J tensile specimens (overall length 25 mm, thickness 0.76mm, gage length 7.6 mm and gage width 1.5 mm) and three TEM disks were prepared for each irradiation condition. For ion irradiation, six TEM disks were mechanically polished down to 1 micron diamond lapping film and shipped

to the Texas A&M University- Radiation effects facility for ion irradiation at the conditions summarized in Table 1. However, due to poor vacuum in the specimen chamber, all the irradiated specimens exhibit a surface contamination layer following irradiation (due in part to outgassing from the silver paste used to attach the specimens to the target holder, and also due to a vacuum leak during the irradiations). The contamination layer formed on the sample surface was relatively non-uniform and the thickness ranged from ~100 nm in 400°C to ~200nm in 700°C. Nanoindentation tests were not performed on the ion irradiated samples as the non-uniform contamination layer will influence the determination of specimen contact area, which may cause errors for the measurement of hardness and modulus. Ion irradiation doses were computed by SRIM following the recommendations of Stoller (40 eV displacement energy, quick Kinchin-Pease option).[7] The calculated ion range is ~1.9 micron and mid-range dose is evaluated at a depth of ~1 micron.

Table 1. Summary of ion irradiation conditions for the high entropy alloy.

Material	Ion irradiation (mid-range dose, ~5.8MeV Ni ions)
HEA (Fe-28%Ni-27%Mn-18%Cr)	1dpa, 500°C
	1dpa, 600°C
	10dpa, 400°C
	10dpa, 500°C
	10dpa, 600°C
	10dpa, 700°C

All the post-irradiation examinations of the neutron irradiated samples were conduced at room temperature. Bulk hardness was measured by a hardness indenter equipped with a Vickers indenter tip. The load and dwell time were set at 500 grams and 10s. Five indents were made on two TEM disks irradiated to 0.1dpa and 1dpa, respectively. Nanohardness was also measured on the same two TEM disks (after light mechanical polishing of the surfaces with 1 micron diamond lapping film) using a Nano Indenter G200, manufactured by Agilent Technologies, with Berkovich diamond indenter. All tests were performed in continuous stiffness measurement mode with a constant load rate $\dot{P}/_{P} = 0.05$ s^{-1}. Nanohardness was measured as a function of depth from the point of contact to a depth of about 1000nm. Hardness data below a depth of ~ 300nm from the surface was discarded due to large data scatter associated with surface roughness. 25 indents were made for each specimen to obtain sufficient statistics for the evaluation of average and error.

Tensile testing was conducted using three SS3J specimens (one control specimen, one 0.1dpa and one 1dpa) on a screw-driven mechanical test frame, with a nominal strain rate of 0.0003s^{-1}. Anomalous strain in the load vs. crosshead displacement data due to machine compliance effects was corrected to show the right stress-strain relationship. The correction was done by assuming that irradiation induces minimum change of elastic modulus, and that Young's modulus is the same for both irradiated and unirradiated samples. Electrical resistivity was measured using a four-point probe technique on five 0.1 dpa and six 1 dpa SS3J tensile specimens. 100 mA current was used through the outer contact near the tab region of the specimen, and the voltage drop between the inner contacts of the specimen's gage section was measured and converted to resistivity based on measurements of the individual sample gage dimensions. For each specimen, five measurements were taken first, and the specimen was then flipped over to make another five measurements to minimize the effect of voltage fluctuation and sample orientation effects.

For the ion irradiated samples, cross-section transmission electron microscopy (TEM) specimens from the irradiated samples were prepared using a focus ion beam (FIB) (FEI Quanta 3D 200i) system with Ga+ ions. The ion energy at the main thinning step is 30keV, and during the later stages of thinning the energy was progressively reduced to 8, 5 and 2 keV with the final thinning at a foil thickness of ~100 nm

performed with a current of 27 pA. In order to minimize the unwanted FIB damage caused by Ga+ ions, a low voltage argon ion polishing system (Fischione NanoMill-model 1040) was subsequently used for creating high quality TEM specimens. A very low voltage and current of 900 eV and 90 pA were used on the TEM specimen during the final thinning. As a final step, a Fischione Plasma Cleaner (Model 1020) was used to remove carbonaceous contamination from the TEM specimen. A Philips CM200 FEG (field emission gun) TEM/scanning transmission electron microscope (STEM) that produces a probe of 1.4 nm at 200-kV operating voltage was used to examine the changes of microchemistry at the grain boundaries in the irradiated samples.

Results and Discussion

The hardness of HEA following neutron irradiation near 70°C increased rapidly at lower dose (0.1 dpa), but the hardness increase slowed down at higher dose (1 dpa). Compared with the unirradiated sample, the bulk hardness of neutron irradiated HEA increased by 80% after 0.1 dpa and by ~120% after 1 dpa (Figure 1). Figure 2 shows the corresponding nanohardness measurement data on the neutron irradiated samples and Figure 3 shows a linear fit of hardness squared as a function of the inverse of indentation depth according to the Nix-Gao model[8] that was used to verify uniform hardness versus depth for the unirradiated and neutron irradiated samples. The R-square values are very close to 1 for all three fitting curves, verifying depth-independent hardness. The nanohardness measurement for neutron irradiated samples showed ~ 70% increase for the 0.1dpa sample and ~80% increase after 1dpa at an indent depth of ~800nm, which was comparable to the bulk Vickers hardness measurement (at an indentation depth ~ 8 to 12 microns, depending on sample hardness). On the other hand, by extrapolation of the Nix-Gao fit in Figure 3, the hardness at infinite depth can be obtained from the intercepts of the curves. The extrapolation showed ~250% hardness increase for 0.1 dpa and ~270% increase for 1 dpa, both higher than the bulk Vickers hardness results.

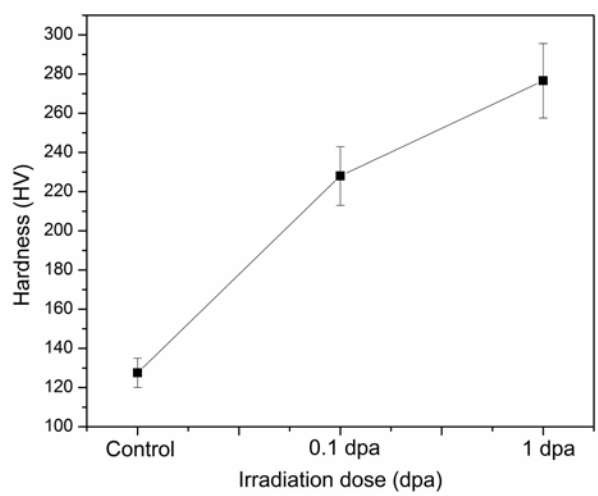

Figure 1. Bulk hardness of neutron irradiated samples as a function of dose

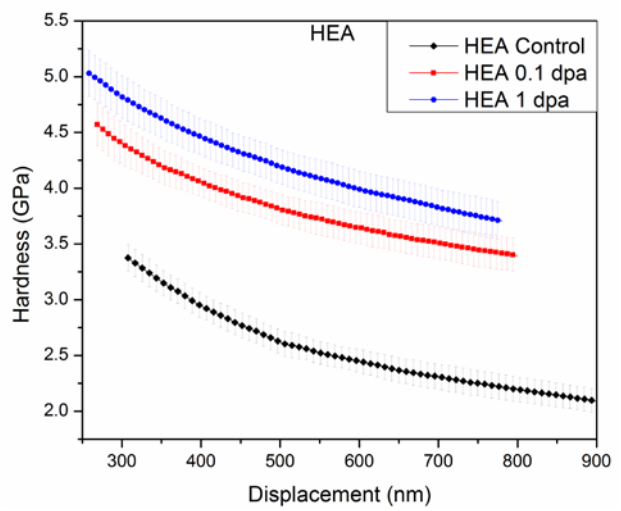

Figure 2. Nanoindentation hardness as a function of depth for samples irradiated by neutrons at 70°C from 0.1 dpa to 1 dpa

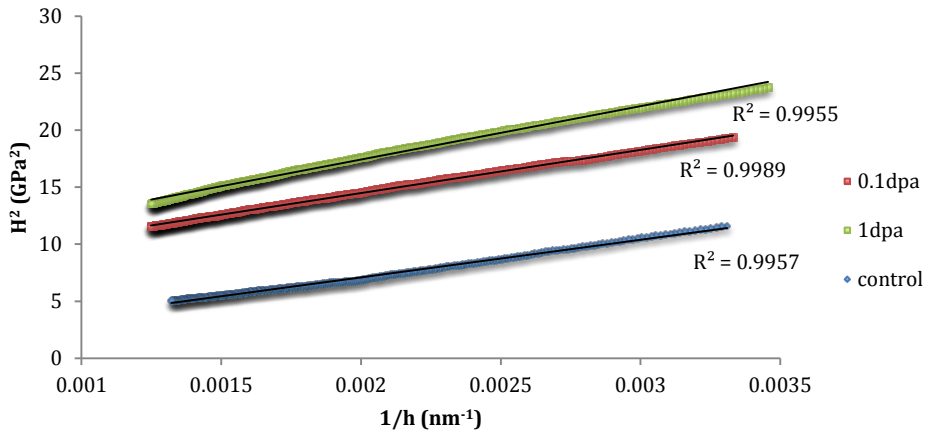

Figure 3. Nix-Gao fit of the nanohardness data, with R-square values below showing the quality of the linear fit

The electrical resistivity of the neutron irradiated samples also increased with irradiation dose (Figure 4). Resistivity increased by ~16% from 0 dpa to 0.1 dpa, but increased only a little (~1% from 0.1 dpa to 1 dpa) with further irradiation dose. For the irradiated alloys, change of electrical resistivity can be caused by precipitate dissolution/formation, phase change, ordering/disordering and defect creation[9], along with nuclear transmutation effects. In the present experiment, the material studied is single phase, and the irradiation is conducted at relatively low dose and at room temperature. Thus, the increase of resistivity should be dominated by production of radiation induced defects. The rapid resistivity increase suggests a large increase in radiation defects from 0 to 0.1 dpa, while the less rapid change of resistivity from 0.1 to 1 dpa indicates slower increase in radiation defects at higher dose regime.

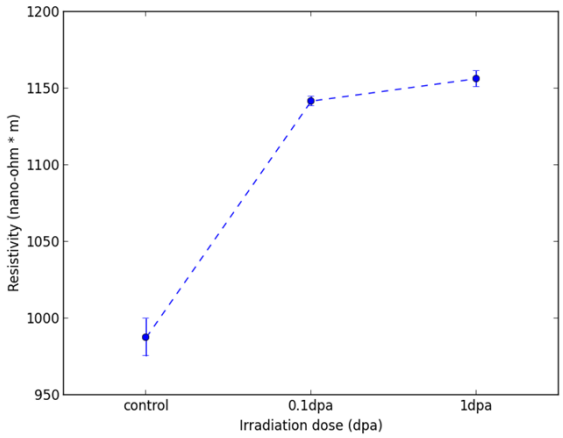

Figure 4. Electrical Resistivity of neutron irradiated samples as a function of dose

Representative stress/strain curves of neutron irradiated high entropy alloy tensile specimens, given in Figure 5, shows similar behavior as typical austenitic 304, 316 and 347 stainless steel[10, 11]. At lower dose, yield strength increases substantially while ductility suffers relatively mild loss. At higher dose, loss of ductility is more significant, but the elongation is still uniform and shows no sign of prompt plastic instability.

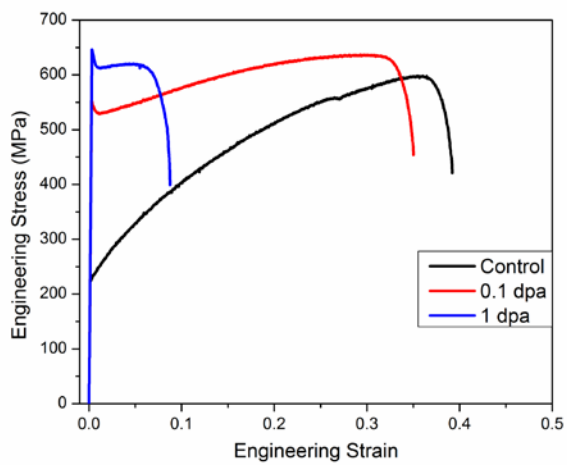

Figure 5. Stress-strain behavior of neutron irradiated tensile samples at different doses

Both irradiated samples exhibit yield drops, and the magnitude of the yield drop increases with dose. The magnitude of yield drop, however, seems to be larger than that of a typical stainless steel. For HEA, the yield drop is ~24 MPa at 0.1 dpa and ~34 MPa at 1 dpa. For 316 stainless steel, the yield drop is ~4MPa at 0.1 dpa and ~16MPa at 0.78 dpa[11].

Both HEA and conventional austenitic alloys exhibit reduction of work hardening with increasing dose, which indicates that neutron irradiation alters the work hardening behavior. However, the magnitude of reduction for HEA is more significant. At 1 dpa, the work hardening regime is almost flat, and the difference between ultimate tensile strength and lower yielding point is only ~8 MPa. The upper yield point is even higher than ultimate tensile strength. This is atypical for austenitic Fe-based alloy (304, 316 and 347) because work hardening can still be observed at relatively high dose[10, 11]. Since plastic deformation is characterized by the interaction of dislocation and pre-existing solute/radiation induced defects (in the

case of austenitic steels, microtwinning is also involved), the differences in yield drop and work hardening magnitude suggest different defect microstructures, or different interaction mode after irradiation.

Since both yield strength and hardness are connected to the plastic properties, change in yield strength should correlate with that of hardness[12]. Previous experimental studies have shown linear correlation between Vickers hardness and yield strength and this correlation is independent of material composition[13]. In this study, the increasing trend of yield strength and hardness also shows good agreement, qualitatively. Yield strength rapidly increases by ~140% from 0 to 0.1 dpa, but the increasing trend slows down and only increases by ~180% from 0 to 1 dpa. This agrees with the trends from Vickers hardness and nanoindentation hardness measurement, showing good consistency between different experiments.

Microstructural examination

Figure 6 shows the over and under focused TEM micrographs of HEA specimen irradiated at 700°C and 10 dpa. The search for void swelling was performed in the midrange damage regions in order to minimize void swelling suppression effects associated with injected ions or the irradiated sample surface. In contrast to conventional Fe-Ni-Cr alloys, HEA shows no pronounced void swelling at any of the ion irradiation conditions in this study. The fact that no voids are found in current HEA after irradiation to midrange doses of 10 dpa at 400-700°C indicates that the HEA has better swelling resistance than conventional austenitic FeCrNi or FeCrMn alloys, which exhibit significant void formation after 10 dpa in this temperature range[14].

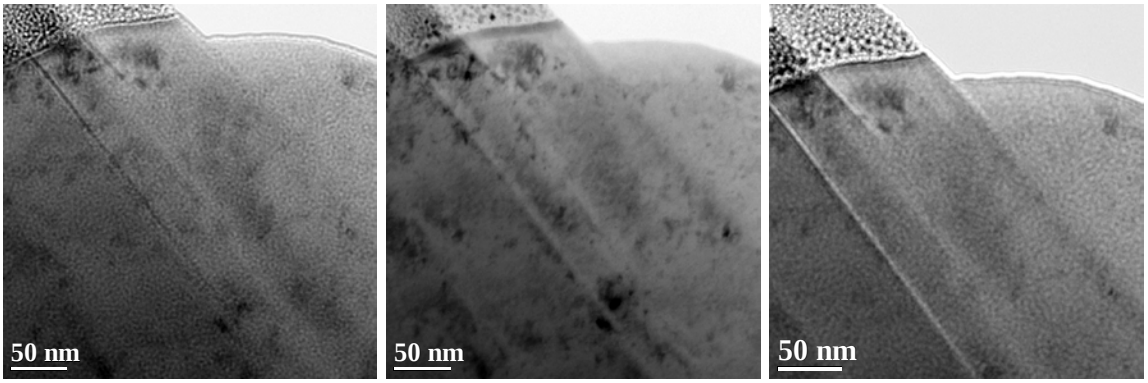

Figure 6. Bright field TEM image series from HEA alloy a) over-focus, b) focus c) under-focus, showing that no voids are observed in the specimen irradiated at 700°C, 10 dpa.

Figure 7 shows the scanning transmission electron microscopy (STEM) micrographs of the samples exposed to different ion irradiation conditions. Samples at any irradiation condition do not show any measurable segregation detectable by STEM/EDS measurements. Figure 7d shows the STEM line profile performed across the grain boundary of 600°C-10dpa specimen, where no variation in composition is observed. This lack of radiation-induced solute segregation (RIS) is in marked contrast to the behavior observed in FeCrNi and FeCrMn austenitic alloys, where Cr and Mn depletion and Ni enrichment have been observed in numerous prior studies[15]. It is assumed that the two main factors that influence the RIS behavior in the current alloy are the composition and high configurational entropy. In high entropy alloys the contribution of configuration entropy in reduction of total Gibbs free energy will be high only when the alloy microstructure is single-phase. Buildup of large local defect concentrations during irradiation can introduce noticeable changes in stability of phases. There would be no RIS if all the vacancies and interstitials created during irradiation are recombined close to where they are created. No measurable segregation in the current HEA suggests that the vacancy-interstitial recombination is high and/or the mobility of vacancies are sluggish even at a relatively high irradiation temperature of 700°C. However, lack of thermodynamic and kinetic databases on HEAs restricts the deeper understanding of their segregation behavior. Nevertheless, it can be clearly concluded that, compared to conventional austenitic

FeCrNi or FeCrMn alloys, a significant difference in radiation response in HEAs at higher irradiation temperatures is observed.

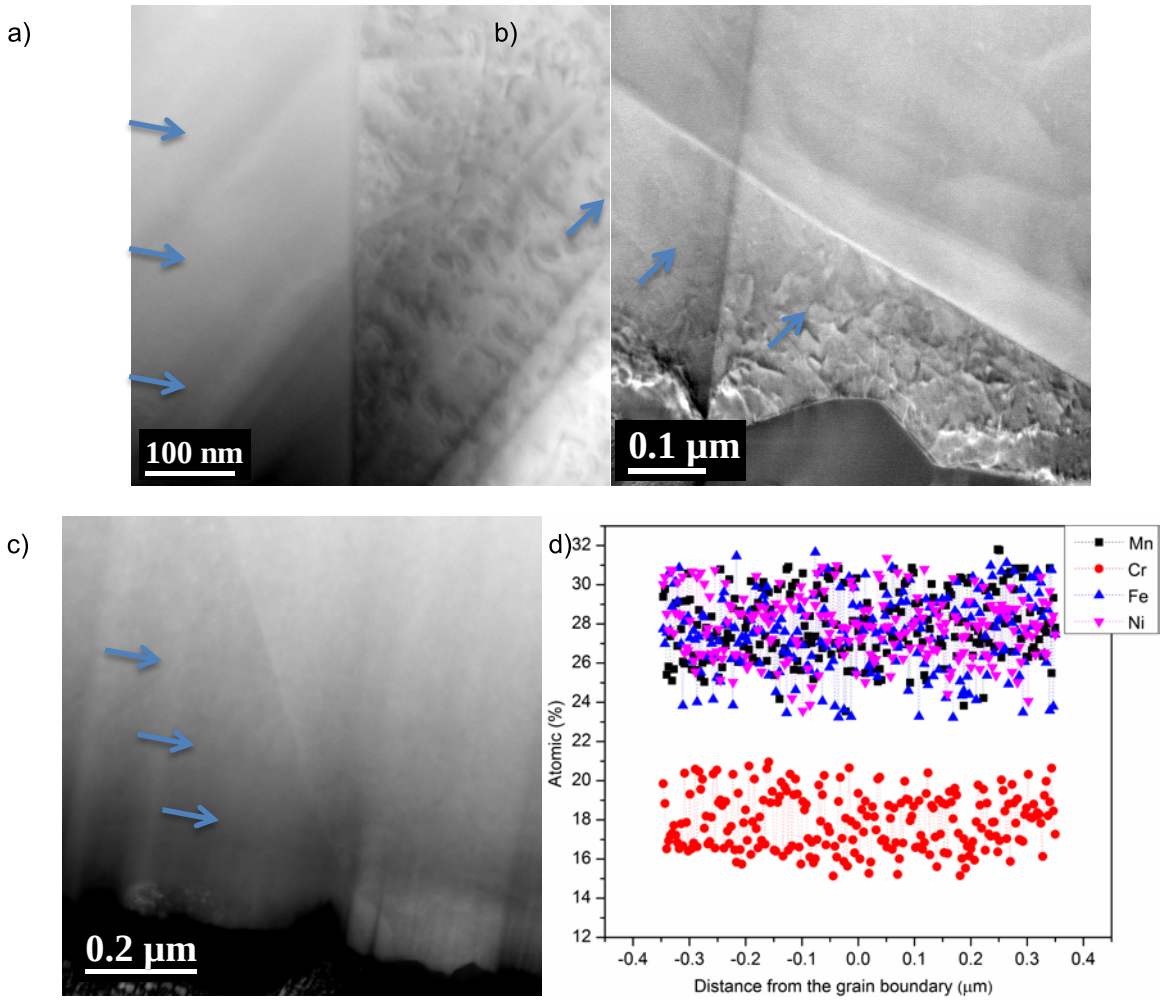

Figure 7. a), b) STEM micrographs showing grain boundaries of 700°C-10dpa specimen, c) STEM micrograph showing grain boundary of 400°C-10 dpa specimen d) STEM/EDS grain boundary composition profile of 600°C-10 dpa specimen.

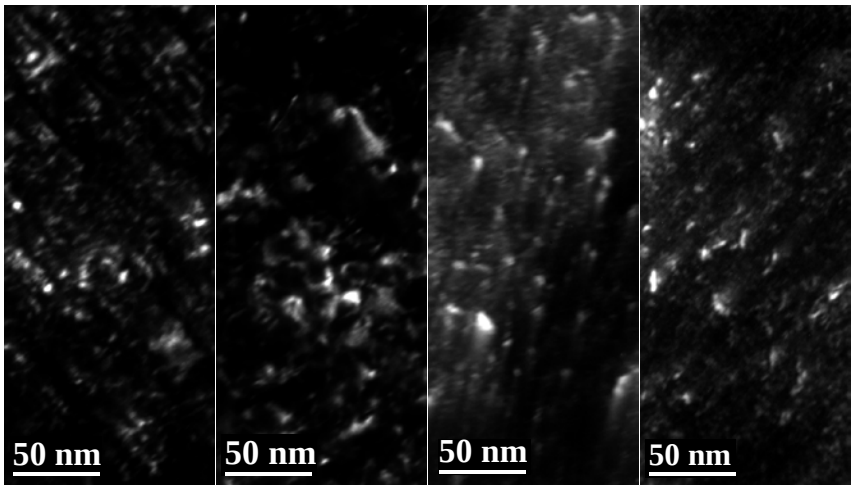

Figure 8. Dislocation loops in weak beam dark field (WBDF) images of 10 dpa irradiated specimens at temperatures a) 400°C, b) 500°C, c) 600°C, d) 700°C.

Figure 8 shows weak-beam dark field images of ion irradiated HEA specimens. Dislocation loops dominate the defect microstructure at all irradiation conditions. Fine scale dislocation loops with diameters ranging from 1 to 10 nm can be seen in the micrographs. Table 2 summarizes the average loop size and loop density variation in HEA with irradiation dose and temperature. A qualitative trend of increase in loop size and decrease in loop density is observed with increasing irradiation temperature. However the increase in dislocation loop size with increasing temperature is not very substantial (from 4 to 5.5 nm as temperature is increased from 400 to 700°C). Loop density appears to nearly saturate after exposure to a dose of 1 dpa at 500°C. Although the uncertainty in loop density measurement is a factor to be considered, it should be noted that the concentration of point defects retained in HEAs in visible defect clusters is around 10^{21}-10^{22} m^{-3}, i.e., about 7 orders of magnitude less than the integrated concentration of point defects produced by the irradiations. The observed defect cluster densities of irradiated HEAs are significantly higher than the reported dislocation loop densities of many Fe-Cr-Ni alloys irradiated under similar conditions, and the corresponding loop sizes for the HEA specimens are smaller than reported for Fe-Cr-Ni alloys[16]. Slight variation in defect density could be due to the fact that some authors separated the black spots and dislocation loops, where in the current study both black spots and dislocation loop are treated as dislocations loops. In addition, if the imaging of loops is done in a thick foil regions (>150 nm), lower loop density is observed due to poor contrast of small (~2 nm) loops and overlap effects. In this study, all the observations were made in relatively thin foils (thickness of 60-80nm). Relatively constant defect density was also observed for high temperature irradiated specimen. Usually, the increase in irradiation temperature results in decrease in loop density and an increase in loop diameter due to increase in diffusion rate of solute interstitial and vacancies. However, the nearly constant dislocation loop density (only a factor of 5 decrease between 400 and 700°C) and limited increase in loop size (17% increase in size between 400 and 700°C) in the ion irradiated HEA specimens suggest that the diffusion kinetics in HEAs is more sluggish than conventional Fe-Ni-Cr alloys. The possibility of relatively low solute diffusivity in HEA alloys is supported by the recent study on Co-Cr-Fe-Mn-Ni high entropy alloy, where it was shown that the HEA showed larger fluctuation in lattice potential sites, which resulted in the presence of abundant low-energy lattice potential sites that would thereby lower the diffusion kinetics of solute atoms[17]. In addition, the smaller loop size in HEA suggest that only a small fraction of the produced point defects are eventually trapped in the loops and recombination of vacancies and interstitials is the dominant recovery process in the HEAs.

Table 2. Summary of microstructural observations in HEAs after ion irradiation

Temperature (°C)	Dose (dpa)	Mean loop diameter (nm)	Loop Density (m^{-3})
400	10	4.66	1.89×10^{22}
500	1	4.13	7.13×10^{21}
500	10	4.32	9.35×10^{21}
600	10	5.21	6.68×10^{21}
700	10	5.45	4.33×10^{21}

References

[1] 1. C. Y. Hsu, J. W. Yeh, S. K. Chen and T. T. Shun, Metallurgical and Materials Transactions a-Physical Metallurgy and Materials Science 35A (5), 1465-1469 (2004).
[2] 2. J. W. Yeh, S. K. Chen, J. Y. Gan, S. J. Lin, T. S. Chin, T. T. Shun, C. H. Tsau and S. Y. Chang, Metallurgical and Materials Transactions a-Physical Metallurgy and Materials Science 35A (8), 2533-2536 (2004).
[3] 3. C. J. Tong, Y. L. Chen, S. K. Chen, J. W. Yeh, T. T. Shun, C. H. Tsau, S. J. Lin and S. Y. Chang, Metallurgical and Materials Transactions a-Physical Metallurgy and Materials Science 36A (4), 881-893 (2005).
[4] 4. Y. J. Zhou, Y. Zhang, Y. L. Wang and G. L. Chen, Applied Physics Letters 90 (18), 3 (2007).
[5] 5. C. M. Lin and H. L. Tsai, Journal of Alloys and Compounds 489 (1), 30-35 (2010).
[6] 6. S. J. Zinkle and G. S. Was, Acta Materialia 61 (3), 735-758 (2013).
[7] 7. R. E. Stoller, M. B. Toloczko, G. S. Was, A. G. Certain, S. Dwaraknath and F. A. Garner, Nuclear Instruments & Methods in Physics Research Section B-Beam Interactions with Materials and Atoms 310, 75-80 (2013).
[8] 8. W. D. Nix and H. J. Gao, Journal of the Mechanics and Physics of Solids 46 (3), 411-425 (1998).
[9] 9. C. Dimitrov, M. D. C. Belo and O. Dimitrov, Journal of Physics F-Metal Physics 10 (8), 1653-1664 (1980).
[10] 10. H. R. Higgy and F. H. Hammad, Journal of Nuclear Materials 55 (2), 177-186 (1975).
[11] 11. K. Farrell, T. S. Byun and N. Hashimoto, Journal of Nuclear Materials 335 (3), 471-486 (2004).
[12] 12. D. Tabor, British Journal of Applied Physics 7 (5), 159-166 (1956).
[13] 13. J. T. Busby, M. C. Hash and G. S. Was, Journal of Nuclear Materials 336 (2-3), 267-278 (2005).
[14] 14. F. A. Garner, H. R. Brager, D. S. Gelles and J. M. McCarthy, Journal of Nuclear Materials 148 (3), 294-301 (1987).
[15] 15. E. A. Kenik, Journal of Nuclear Materials 205, 317-323 (1993).
[16] 16. S. J. Zinkle, P. J. Maziasz and R. E. Stoller, Journal of Nuclear Materials 206 (2-3), 266-286 (1993).
[17] 17. K. Y. Tsai, M. H. Tsai and J. W. Yeh, Acta Materialia 61 (13), 4887-4897 (2013).